Soil Moisture Content Inversion by Coupling AEA and ARMA

Yanling FENG [1], Junli NIE [1], Guoqing XIE [2], Heng LV [3]

[1] Dept. of Key Laboratory of Karst Georesources and Environment (Guizhou University), Ministry of Education, Guizhou University, Jiaxiunan Road 515, 550025, Guiyang, China
[2] Dept. of Hydraulic Power Survey and Design Institute Co., Ltd, Minzhu Road 1-5, 530022, Nanning, China
[3] Dept. of Mineral Exploration Institute, Bureau of Geology and Mineral Resources of Gansu Province, Langongpin Road 121, 730050, Lanzhou, China

2621486711@qq.com, 42264008@qq.com, 1309544042@qq.com, 918615761@qq.com

Submitted March 8, 2024 / Accepted May 21, 2024 / Online first June 7, 2024

Abstract. *This study aimed to explore the inversion method of soil moisture content by using numerical simulation and field detection. The researchers used the early signal amplitude envelope (AEA) method to directly invert soil moisture in the shallow part of the soil, which avoided the transmission error of the Topp formula. The Auto-Regressive Moving Average Model (ARMA) was used to calculate the power spectrum of radar signals, and the BP neural network was used to train the power spectrum of different Gaussian windows, so as to improve the inversion accuracy. According to the study, the average error of soil moisture content inverted by AEA method was 0.45% in the range of 0–0.41 m, while the error of ARMA method in depth range of 0.1–1.0 m was less than 1%. The results showed that the combination of the two methods can effectively invert the soil moisture content within the radar detection range.*

Keywords

Ground penetrating radar, AEA, ARMA, soil moisture content, BP neural network

1. Introduction

Accurate acquisition of soil water information plays an important guiding role in the fields of ecohydrology, soil science, engineering geology, and agronomy [1], [2], [3], [4]. Ground Penetrating Radar (GPR) is a rapid, non-destructive detection technology known for its high resolution and in-situ capabilities [5]. GPR technology relies on differences in dielectric properties of underground materials, with the dielectric constant being closely linked to the water content in the medium. As a result, GPR is extensively utilized for detecting soil moisture content at the mesoscale [6], [7], [8].

In general, the methods of GPR to detect soil moisture content can be divided into time domain and frequency domain methods. In terms of the time-domain method, the most widely used method is the ground wave method. At the earliest, people used the common center point method to calculate the dielectric constant of underground media, and then used the empirical formula of medium moisture content. For example, Koyama et al. [9] proposed a method to estimate the soil moisture profile in the vertical direction from multi-offset radar data, and used the common center point method to obtain the dielectric constant and depth of the reflected soil layer. Ercoli [10] employed both indoor and outdoor studies to estimate the moisture content of two extensively exposed sandy soils in central Italy. To determine the subsoil moisture content in the unsaturated zone, they also examined the ground wave's two-way time travel velocity. Since then, the method proposed by Pettinelli [11] to use the Average Envelope Amplitude of the early signal of the radar wave has been gradually applied to the time-domain method, which no longer needs to separate the ground wave from the radar signal, and directly uses the amplitude envelope of the early signal to obtain the dielectric constant. By applying the AEA method to extract the average amplitude envelope of the early signal of the radar wave, some researchers [12], [13], [14] were able to acquire soil moisture content that was comparable to the Time Domain Reflectometer's detection accuracy. Then the scholars [15], [16] combined numerical simulation and field detection methods to verify the relationship between the ground wave amplitude and soil permittivity, and to demonstrate that the AEA method can accurately and reliably invert soil moisture content. Calculation of soil permittivity, however, requires first determining the ground wave velocity, then the soil moisture content according to the Topp formula. In addition, the propagation depth of ground waves is limited when the amplitude analysis is carried out, so that the detection depth of AEA in detecting soil moisture content is relatively limited.

In the study of the frequency domain method, Wu [17] applied the full waveform inversion of ground penetrating radar to soil moisture mapping and accurate irrigation of potato fields. Laurens [18] analyzed the radar signal spectrum of concrete with different moisture contents, and found that the change of concrete moisture content would lead to electromagnetic dispersion, and the peak main frequency would be shifted. A. Benedetto [3] used GPR frequency domain

DOI: 10.13164/re.2024.0376

signals to estimate the water content of different types of unsaturated soils, and found that when the soil contains clay, the spectral shape of the reflected GPR signal changes uniformly with the increase of water content, so it is pointed out that there is a certain relationship between the change of soil water content and the frequency change of radar waves. Subsequently, some researchers [19] combined GPR numerical simulation and full waveform inversion methods to explore the significant impact of shallow soil moisture stratification on radar data. Pongrac [20] used a multiscale triangulation filter to process the power spectrum of the GPR response, considering the soil conditions as dry, wet, and heterogeneous, and using the Relief F algorithm for sorting. However, when studying the relationship between the frequency peak shift of the GPR spectrum and soil water, it only has a significant effect on high-resolution signals, and the GPR power spectrum is also affected by low resolution, so it is necessary to consider the influence of multiple GPR power spectra on soil moisture content. Yang Feng [21] used the Auto-Regressive Moving Average Model for the first time to study the influence of soil moisture changes on radar power spectrum, and this method has been widely used. Researchers like Cui et al. [22] utilized the ARMA power spectrum estimation technique to analyze radar data, examining sandy soil distribution with varying compaction levels and water contents. Subsequently, other scholars [23], [24], [25] extracted the radar wave power spectrum on this basis to accurately and quickly predict the soil moisture content of loam and clay to verify the reliability of the method. Tang et al. [26] further enhanced measurement accuracy by establishing the ARMA radar dynamic test model. However, when using the power spectrum attribute to detect soil moisture content, it is limited by the principle of the algorithm [27], which makes the calculation error in the soil depth range corresponding to the length of the first rolling half-time window large, and the inversion of moisture content in the shallow part of the ground surface is not accurate enough.

In summary, there is an urgent need to find a method to efficiently invert soil moisture content in the entire radar detection depth range. Therefore, on the basis of previous researches, considering the advantages of AEA and ARMA, this paper uses GPR numerical simulation method combined with BP neural network to invert the volumetric moisture content of soil. In order to test the feasibility of the two methods for inverting soil moisture content from common offset radar data, this field survey provides a new idea for the ground penetrating radar to accurately invert soil moisture content within its detectable depth range.

2. Research Methods

2.1 Study on AEA Inversion Method of Soil Moisture Content

When GPR works, the amplitude of the radar wave is affected by the electromagnetic wave properties of the surrounding medium, and its amplitude A decreases exponentially relative to the initial amplitude A_0 with the increase of the propagation depth h. Instant (1)

$$A = A_0 \, \mathrm{e}^{-\alpha h} \tag{1}$$

where α is attenuation constant, $\alpha = \frac{\sigma}{2}\sqrt{\frac{\mu}{\varepsilon_\mathrm{r}}}$; σ is electrical conductivity (S/m), μ is permeability (H/m), ε_r represents relative permittivity. The relative permittivity of water is 81, and the soil permittivity is generally 3–25, so the relative permittivity is mainly controlled by the moisture content and has an obvious influence on the amplitude.

In order to use the AEA method to invert soil volumetric moisture content, the open-source software GPRMax [28] was used to simulate the forward simulation of GPR. A two-dimensional uniform moisture content model (Tab. 1 for model parameters) was established, and two frequency antennas were selected to simulate eight groups of soils with different moisture contents, in which the soil volumetric soil moisture content was 5%, 10%, 15%, 20%, 25%, 30%, 35% and 40%, respectively. The forward simulation is carried out by using the common offset method, so as to obtain the radar profiles corresponding to different soil moisture content.

The single-channel signal amplitude was extracted from the simulated radar profiles of 8 groups of different soil moisture contents. Then perform the Hilbert transformation according to (2):

$$H(t) = x(t) \times h(t) = \frac{1}{\pi} \int_{-\infty}^{+\infty} \frac{X(\tau)}{t-\tau} \mathrm{d}\tau \tag{2}$$

where $x(t)$ represents raw signal of GPR, $h(t) = x(t)/(\pi t)$ is treated as the real part and $H(t)$ as the imaginary part to construct an analytic signal as (3):

$$f(t) = x(t) + \mathrm{j}H(t). \tag{3}$$

The amplitude envelope is as follows:

$$E(t) = |f(t)| = \sqrt{x^2(t) + H^2(t)}. \tag{4}$$

The GPR single-channel signal was made simpler by the positive amplitude envelope that resulted. The average amplitude envelope value of the radar wave was then determined by selecting 20 single-channel data points for each group and calculating the amplitude envelope value of the first positive half-cycle of the radar wave.

2.2 Study on the Effective Detection Depth of the AEA Method

In order to clarify the effective detection depth of soil moisture content detected by AEA method, a model of dry and wet layered soil medium with uniform soil moisture content in the layer was established, with a size of 2 m × 1 m (as shown in Fig. 1). The top green layer of the model was air, the layer thickness was 0.4 m, the relative permittivity

Antenna [MHz]	The dimensions of the model [m × m]	Transmit and receive antenna distance [m]	Sampling time window [ns]	Grid differential step size [m]
200	4 × 2	0.8	60	0.01
400	2 × 1	0.4	30	0.005

Tab. 1. Model parameters.

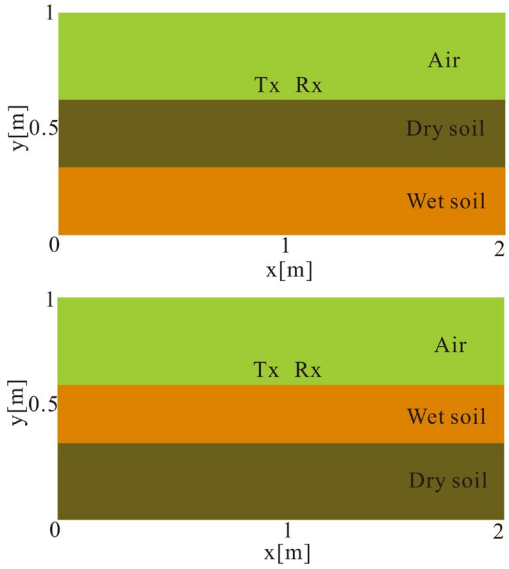

Fig. 1. Schematic diagram of the two-layer soil model.

was 1, the volume moisture content of the dry soil layer was 5%, the volume moisture content of the wet soil layer was 35%, and the magnetic permeability of all media in the model was the same as that of air. The established layered model was numerically simulated using the finite difference time domain (FDTD) approach. The detection was simulated using the common center point method (CMP), with the model parameters being identical to those listed in Tab. 1.

By altering the thickness of the upper layer of soil incrementally and running simulations repeatedly, the variations in ground wave velocity were observed. Through velocity analysis methods, the corresponding ground wave velocities for different soil layers were determined. Specifically, the ground wave velocity changes with the change of the upper soil thickness, but with the increasing thickness of the upper layer, the ground wave velocity decreases and gradually stabilizes under the influence of the lower soil layer, that is, as the thickness of the upper layer increases to a certain value, the ground wave velocity will no longer be affected by the lower soil layer, and the critical value of the corresponding upper layer thickness is regarded as the effective detection depth of the ground wave in the soil [29].

The simultaneous wavelength (5), wave velocity (6) and Topp empirical formula (7) were used to obtain the corresponding wave velocity changes of soil with different layer thicknesses, and the relationship between soil moisture content and effective detection depth was analyzed.

$$\lambda = \frac{c}{f\sqrt{\varepsilon_r}}, \tag{5}$$

$$v = \frac{\lambda}{t}, \tag{6}$$

$$\theta = -5.3\times10^{-2} + 2.92\times10^{-2}\varepsilon_r - 5.5\times10^{-4}\varepsilon_r^{\,2} + 4.3\times10^{-6}\varepsilon_r^{\,3} \tag{7}$$

where λ denoted the wavelength (m), c was the speed of light propagation in a vacuum (m/s), f stands for frequency (Hz), v displays wave velocity (m/s), t was for round-trip travel (s), θ characterized soil volumetric moisture content (%).

2.3 Optimization of Power Spectral Attributes

Using the radar profile data of Sec. 2.1 numerical simulation, the AR power spectrum model was used to extract the radar signal power spectrum and obtain the characteristic parameters of the power spectrum attributes. Then, each power spectrum attribute parameter was fitted with soil moisture content, and the power spectrum attribute parameters were optimized and selected by the cross-correlation algorithm, and the power spectrum attribute parameters that were highly correlated with the moisture content and independent of each other were selected.

ARMA(p,q) can be expressed as:

$$X_t = c + \varepsilon_t + \sum_{i=1}^{p}\varphi_i X_{t-i} + \sum_{j=1}^{q}\theta_j\varepsilon_{t-j} \tag{8}$$

where p and q were the autoregressive order and moving average order of the model; φ and θ were undetermined coefficients that were non-zero; ε_t independent error term, i.e., white noise WN(0,σ^2); X_t was a stationary, normal, zero-mean time series. It can be rewritten in the lag operator notation [30] as:

$$\left(1-\sum_{i=1}^{p}\varphi_i L^i\right)X_i = \left(1+\sum_{i=1}^{q}\theta_i L^i\right)\varepsilon_t \text{ or } \varphi(L)X_t = \theta(L)\varepsilon_t. \tag{9}$$

If $\varphi(L) = 1$, then the process of (9) is MA(q), and if $\theta(L) = 1$, then Equation (9) was called AR(p), so the autoregressive moving average model was divided into three categories: AR model, MA model and ARMA model. The AR model was a linear equation that can be equivalent to predicting the model, so the AR model was selected to extract the power spectral attributes of radar signals.

First, the input was white noise in the model, and the difference equations and system functions of the p-order AR model were as follows:

Attribute category	Parameter	Definition	Formula
Frequency domain attributes [MHz]	The main Frequency	The frequency at which the power spectrum curve achieves its maximum value.	$f_{max}=f_{Pmax}$
	Center frequency	The frequency at which the power spectrum energy is half of the total energy.	$f_m=f_{½E}$
	Frequency of the center of gravity	The power spectral amplitude is used as the weights and the frequency is the weighted average.	$f_c=\frac{\int_0^{+\infty} fP(f)\mathrm{d}f}{\int_0^{+\infty} P(f)\mathrm{d}f}$
	Weighted power frequency	Reach the frequency at 1/2 of the full band frequency-weighted power spectrum.	$f_h=\frac{1}{2}\int_0^{+\infty} f\lvert P(f)\rvert^2\,\mathrm{d}f$
	Root mean square frequency	The square of the signal frequency is a weighted average, with the power spectral amplitude as the weight and the arithmetic square root.	$R_{msf}=\sqrt{\frac{\int_0^{+\infty} f^2P(f)\mathrm{d}f}{\int_0^{+\infty} P(f)\mathrm{d}f}}$
	Edge frequencies	A frequency at which the signal power distributed from 0 Hz to that frequency is 95 per cent of the total signal power.	$0.95E=\int_0^{f_e}\lvert P(f)\rvert\mathrm{d}f$
Energy attributes [dB]	Band energy	The total area of the power spectrum over the bandwidth.	$E=\int_0^{+\infty}\lvert P(f)\rvert\mathrm{d}f$
	Clock energy	The amplitude corresponding to the frequency at which the power spectrum curve obtains its maximum value.	$E_{pf}=\lvert\max(P(f))\rvert$
Aggregation degree attribute	Power spectral entropy	The power spectrum values are summed by multiplying the product of their negative logarithms.	$H_f=-\sum_{n=0}^{N}P(n)\log P(n)$
	Standard deviation of frequency（MHz）	The square of the difference between the power spectrum frequency and the center of gravity frequency is the weighted average, with the power spectrum amplitude as the weight and the arithmetic square root.	$R_{vf}=\sqrt{\frac{\int_0^{+\infty}(f-Fc)^2P(f)\mathrm{d}f}{\int_0^{+\infty}P(f)\mathrm{d}f}}$
Energy distribution attributes	Bandwidth energy percentage	The ratio of a single band to the total band power spectrum, which has a maximum value of 1 and a minimum value of 0.	$BEP=\frac{\sum_{f_i=f_{WL}}^{f_{WH}}\lvert P(f_i)\rvert}{\int_0^{+\infty}\lvert P(f)\rvert\mathrm{d}f}$

Tab. 2. Power spectrum parameter attributes [25].

$$x(n)=-\sum_{i=1}^{p}a_i x(n-i)+\omega(n), \tag{10}$$

$$H(z)=\frac{1}{A(z)}=\frac{1}{1+\sum_{i=1}^{p}a_i\,\mathrm{e}^{-\mathrm{j}\omega t}}. \tag{11}$$

The signal $Y(n)$ output by the signal $X(n)$ after being processed by the system $H(z)$ had the following relationship:

$$P_x\left(\mathrm{e}^{\mathrm{j}\omega}\right)=\frac{\sigma^2}{\left|1+\sum_{i=1}^{p}a_i\,\mathrm{e}^{-\mathrm{j}\omega k}\right|}. \tag{12}$$

Then the power spectrum output of the model was:

$$P_{xx}\left(\mathrm{e}^{\mathrm{j}\omega}\right)=\sigma_\omega^2\left|H\left(\mathrm{e}^{\mathrm{j}\omega}\right)\right|^2=\sigma_\omega^2\left|\frac{1}{1+\sum_{i=1}^{p}a_i\,\mathrm{e}^{-\mathrm{j}\omega t}}\right|. \tag{13}$$

The relationship between the model parameter a_k and the autocorrelation function $x_m(m)$ of $x(n)$ was as follows:

$$r_x(m)=\begin{cases}-\sum_{i=1}^{p}a_i r_x(m-i), m\geq 1,\\ -\sum_{i=1}^{p}a_i r_x(i)+\sigma^2, m=0.\end{cases} \tag{14}$$

The ground penetrating radar data of the uniform soil moisture content model obtained by zero correction were carried out to extract the single-channel signal. The optimal order was calculated by using the Akaike information criterion [31] to calculate the radar signal power spectrum of soils with different moisture contents, as shown in Fig. 2 (taking 400 MHz as an example), where the abscissa was the frequency (MHz) of the GPR power spectrum and the ordinate was the energy (dB).

It can be seen from Fig. 2 that with the increase of soil moisture content, the power spectral energy of the GPR signal

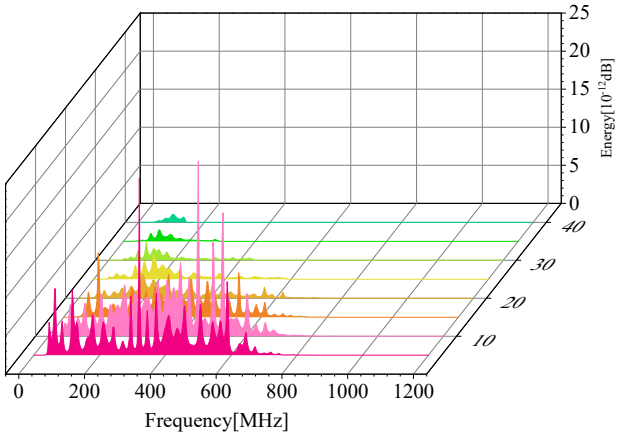

Fig. 2. Radar wave signal power spectrum of different soil moisture content at 400 MHz.

gradually decreases, and the frequency band distribution gradually shifts to the low frequency and gradually gathers. Therefore, the higher the soil moisture content, the smaller the total energy of the power spectrum of the reflected wave.

The power spectrum attribute parameters of radar signals corresponding to various soil moisture contents were computed using the power spectrum attribute calculation formula (Tab. 2). Also, cross-correlation was adjusted by analyzing the relationship in turn between each power spectrum attribute parameter and soil moisture content.

2.4 Rolling Spectrum Profiling Technique

In order to obtain the soil moisture content at different depths, a Gaussian window was added to the radar signal [21] to analyze the spectral local characteristics of the corresponding signals of the soil at different depths. The function of the window property satisfied the condition of (15):

$$\omega G(\omega), tg(t) \in L^2(R). \tag{15}$$

In the formula, $g(t)$ was the window function, $G(\omega)$ was the Fourier transformation of $g(t)$. $g(t)$ was selected to meet the following relationships:

$$4\Delta_{g(t)}\Delta_{G(\omega)} \geq 2. \tag{16}$$

When the $g(t)$ is the Gaussian function, the equal number is established. It can be seen that the Gaussian window is the best window for local analysis.

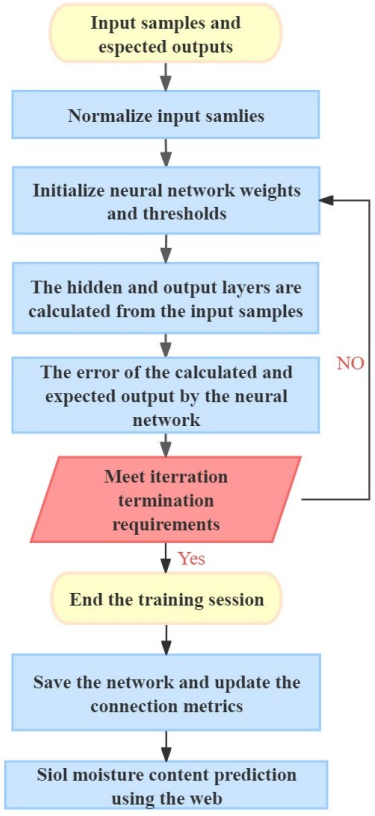

Fig. 3. Flow diagram of BP neural network inversion of soil moisture content.

$$g_a(x) = \frac{1}{2\sqrt{\pi a}} e^{-\frac{x^2}{4a}}, a > 0 \cdot \tag{17}$$

At this point, the power spectrum of the radar signal in each time window can be obtained.

2.5 BP Neural Network Inverts Soil Moisture Content

BP neural networks have powerful learning, memory, fault tolerance, nonlinearity, and adaptive capabilities, which can achieve input-to-output mapping by repeatedly learning large amounts of data. The networks used in this study are mainly divided into input layer, hidden layer and output layer. When the input layer samples propagate forward in the neural network, the obtained output value is compared with the expected output, so that the error is continuously back propagated, thereby changing the connection weight between the neurons in the hidden layer. The output of the final input sample through the neural network is consistent with the actual output. The inversion process is shown in Fig. 3.

3. Results and Analysis

3.1 The Results of the AEA Method

The reciprocal envelope of the early signal amplitude of the ground wave corresponding to the soil moisture content of the eight groups with different soil moisture content was fitted to the soil volume moisture content, and the results were shown in Fig. 4. Considering the influence of different frequency antennas, the amplitude envelope values of 200 MHz and 400 MHz antenna signals were normalized. Equation (18) is the fitting relation. It can be seen from the figure that there was an obvious linear relationship between the reciprocal envelope of the early signal amplitude and the soil moisture content.

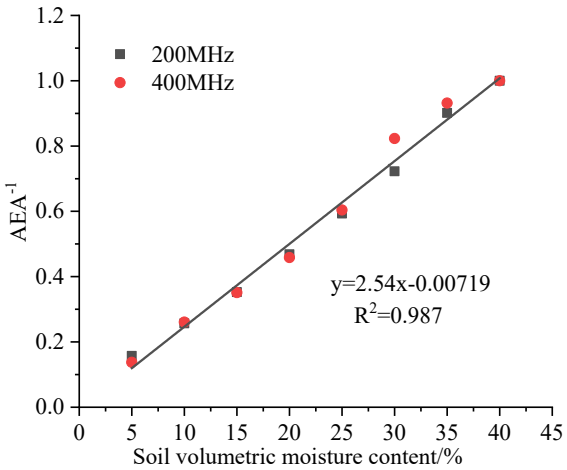

Fig. 4. Fitting relationship between the reciprocal envelope of radar wave amplitude and soil volume moisture content after normalization.

3.2 The Effective Depth Detection Result

The velocity analysis of the radar profiles collected by the 200 MHz and 400 MHz antennas was carried out sequentially. The propagation velocity of the ground wave in different layers of soil thickness was calculated (Fig. 5). It can be seen from Fig. 5 that when the upper soil was dry, with the increase of the thickness of the dry soil layer, the ground wave velocity increased first and then smoothly. When the upper soil layer is wet, the thicker the wet soil layer, the ground wave velocity decreased first and then stabilized. The ground wave velocity corresponding to the 400 MHz antenna reaches equilibrium first, indicating that the larger the antenna, the shallower the effective detection depth. The effective detection depths of the 200 MHz antenna in the dry and wet soil model were 0.41 m and 0.20 m, and the effective detection depth of the 400 MHz antenna in the dry and wet soil was 0.24 m and 0.13 m.

According to (5), the wavelength of the ground wave corresponding to the soil detected by the antenna at different frequencies is calculated, and the effective detection depth and wavelength are linearly fitted to obtain $h = 0.46\lambda + 0.046$ ($R^2 = 0.9859$). Combined with (7) to fit the relationship between soil volume moisture content and the effective detection depth of ground waves, it is represented as Fig. 6, with the increasing soil moisture content, the effective detection depth of ground waves decreases exponentially. It can also be seen that soil moisture content was an important factor affecting the ground wave signal.

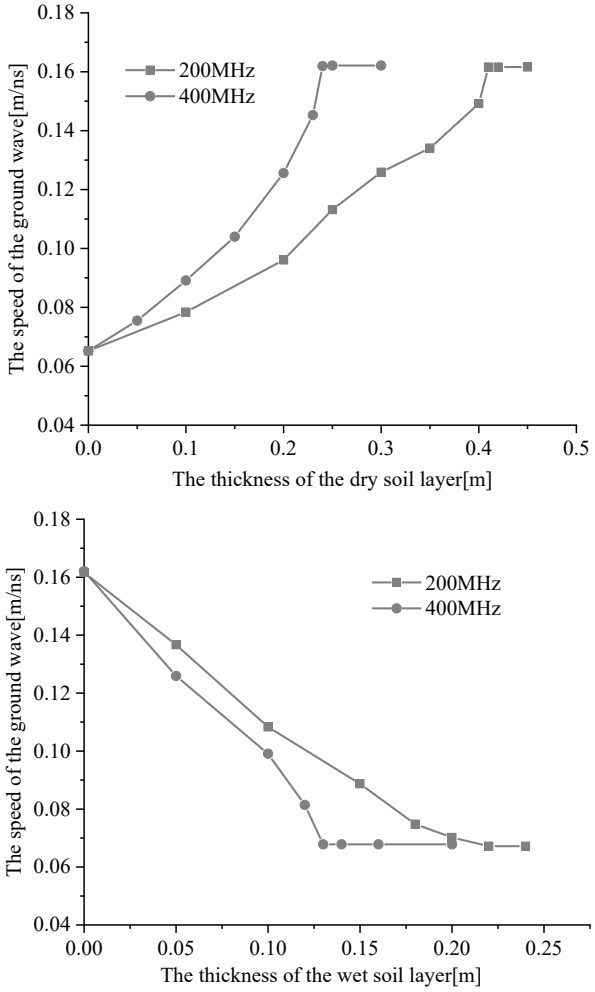

Fig. 5. Propagation velocity curves of ground waves in the double-layer soil model when the thickness of the upper soil changes.

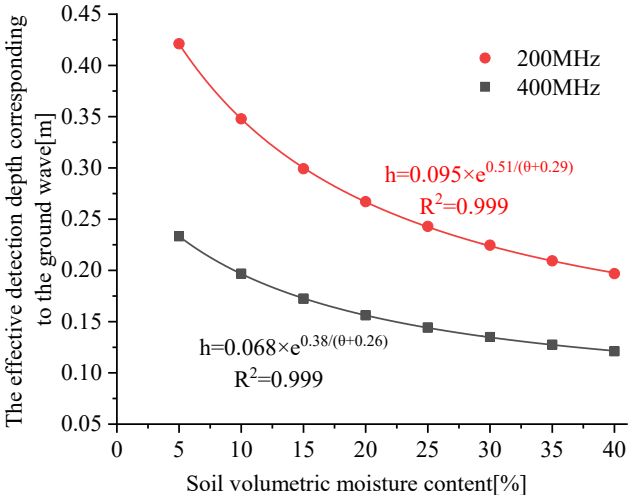

Fig. 6. Relationship between the effective detection depth of ground wave and different soil moisture content.

3.3 The Results of ARMA Combined with BP Neural Network

Table 3 shows the correlation coefficients between the GPR power spectrum attribute parameters and the soil moisture content.

The power spectrum attribute with a large correlation coefficient greater than 0.9 with moisture content is selected for cross-correlation calculation, and the cross-correlation relationship is shown in Fig. 7.

From Fig. 7, the attribute parameters with a correlation value greater than 0.98 and a significant positive correlation at the level of 0.01 are selected to optimize the dimensionality reduction of the attribute parameters. Finally, the main frequency, center frequency, frequency of the center of gravity, band energy, standard deviation of frequency, band energy share 0–200 MHz, band energy share 200–300 MHz were selected as the power spectrum attribute parameters of the 200 MHz antenna, and the main frequency, frequency of the center of gravity, standard deviation of frequency, edge frequencies, band energy, band energy share 0–400 MHz, band energy share 400–600 MHz were selected as the power spectrum attribute parameters of the 400 MHz antenna.

According to the effective detection depth and formation electromagnetic wave velocity obtained by the AEA method, the effective time window was calculated. The Gaussian window length was determined by increasing the formation velocity and the maximum measurable depth by 30% of the time window. The rolling spectrum profile technique was used to intercept GPR signals within a range of about 20 ns, with a window length of 2 ns and a depth of

Power spectrum properties	R_{200}	R_{400}	Power spectrum properties	R_{200}	R_{400}	Power spectrum properties	R_{200}	R_{400}
Main frequency [MHz]	0.93	0.92	**Standard deviation of frequency[MHz]**	0.93	0.94	**Band energy share 0–200 MHz**	0.97	0.88
Center frequency [MHz]	0.91	0.97	**Edge frequencies [MHz]**	0.92	0.91	**Band energy share 0–400 MHz**	0.88	0.96
Frequency of the center of gravity [MHz]	0.93	0.95	**Band energy share 0–100 MHz**	0.83	0.6	**Band energy share 0–600 MHz**	0.83	0.84
Band energy [MHz]	0.98	0.99	**Band energy share 100–200 MHz**	0.89	0.92	**Band energy share 200–400 MHz**	0.89	0.57
Clock energy [MHz]	0.86	0.85	**Band energy share 200–300 MHz**	0.91	0.19	**Band energy share 400–600 MHz**	0.84	0.96
Power spectral entropy [MHz]	0.88	0.89	**Band energy share 300–400 MHz**	0.9	0.82	**Band energy share 100–600 MHz**	0.75	0.4
Weighted power spectrum frequency [MHz]	0.64	0.76	**Band energy share 400–500 MHz**	0.91	0.92	**Band energy share 200–500 MHz**	0.82	0.74
Root mean square frequency [MHz]	0.76	0.97	**Band energy share 500–600 MHz**	0.75	0.84	/	/	/

Tab. 3. Correlation coefficient between power spectrum attribute parameters and moisture content.

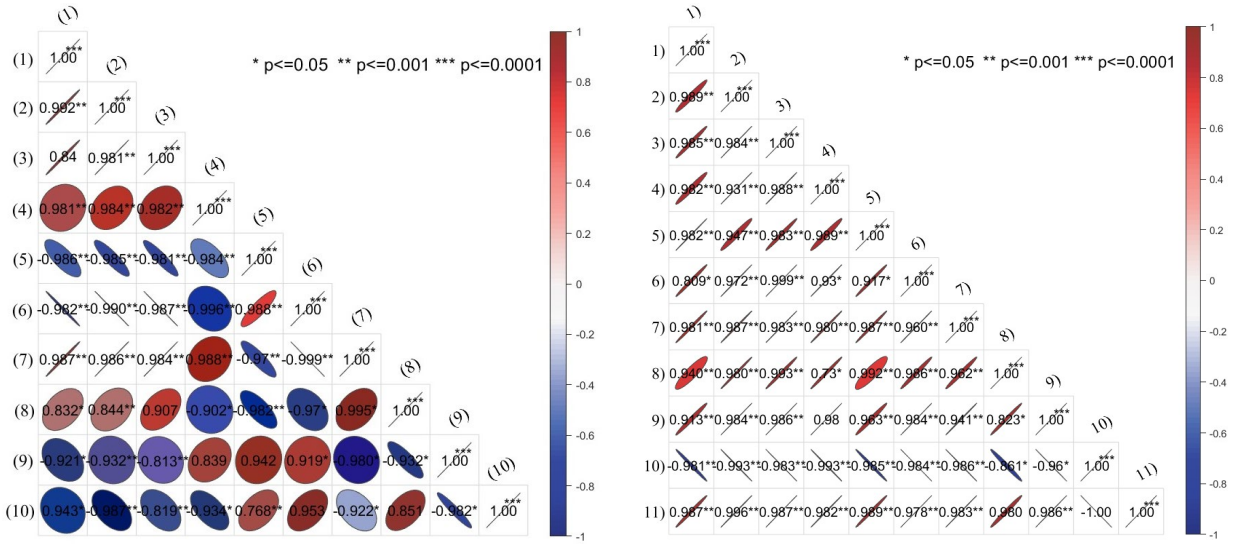

Fig. 7. Cross-correlation of power spectrum attribute parameters (200 MHz left, 400 MHz right).

Notes:
(1)~(10) indicates the main frequency, center frequency, frequency of the center of gravity, band energy, standard deviation of frequency, band energy share 0–200 MHz, band energy share 200–300 MHz, edge frequencies, band energy share 300–400 MHz, band energy share 400–500 MHz of the 200 MHz frequency antenna in turn;
1)~11) indicates the main frequency, center frequency, frequency of the center of gravity, band energy, standard deviation of frequency, root mean square frequency, edge frequencies, band energy share 100–200 MHz, band energy share 400–500 MHz, band energy share 0–400 MHz, band energy share 400–600 MHz of the 400 MHz frequency antenna in turn.

0.1 m for each segment. A total of 480 sample data of soil moisture content samples at different depths in eight groups of simulation experiments were selected as the training set of neural network. Initially, the input layer nodes, hidden layer nodes, and output layer nodes were 7, 7, and 1 respectively to build the network. The training set was used to train the built network, and finally the number of implied layers and nodes in the implied layer was determined to be 3 layers, 6 nodes, and the learning efficiency was 0.1, and the best effect was achieved when the training time was 1000 times. The data obtained from the simulation was returned to the original order of magnitude using the trained model. The output showed the error between the true value and the anticipated value.

Figure 8 shows the comparison of the predicted and measured moisture content of the BP neural network, the average absolute errors of the 200 MHz and 400 MHz antennas predicted and the actual moisture content were

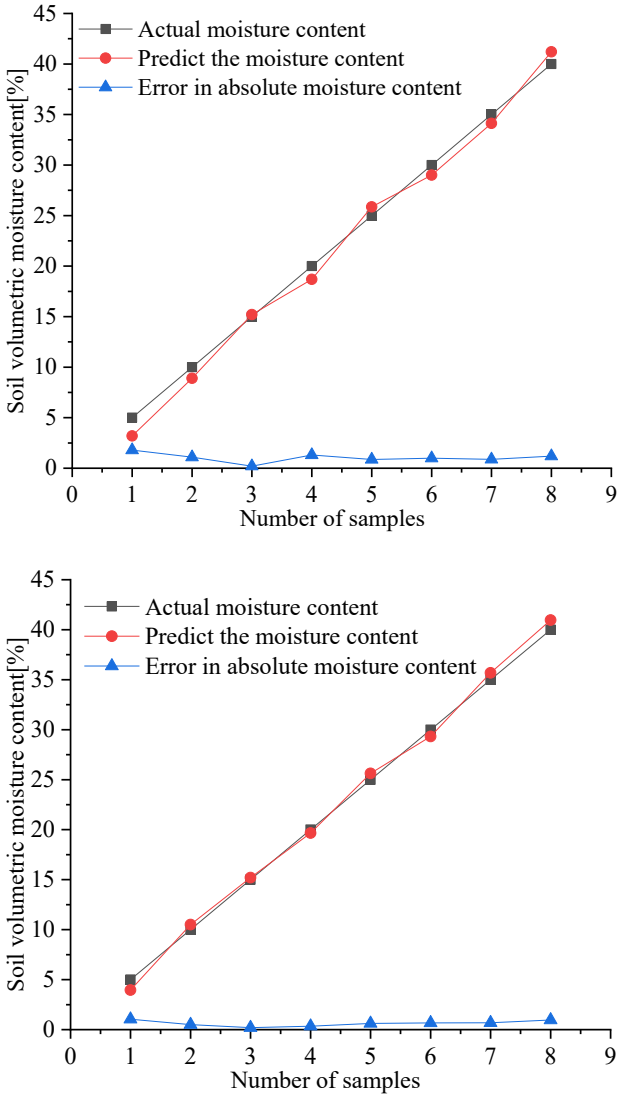

Fig. 8. Comparison of neural network prediction and actual soil moisture content (200 MHz above, 400 MHz below).

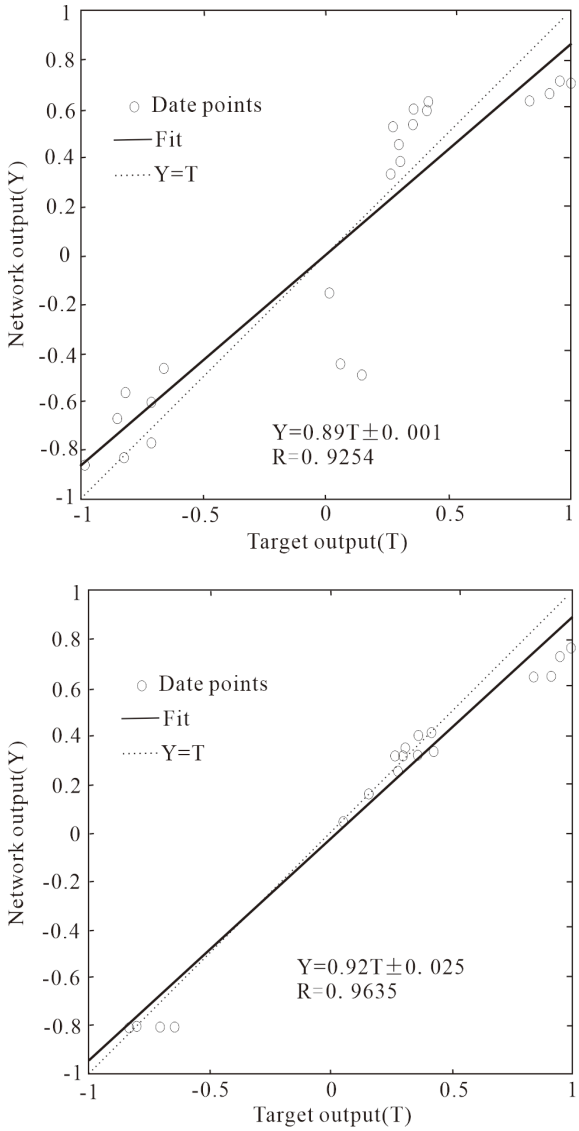

Fig. 9. Ground penetrating radar neural network outputs regression lines (200 MHz above, 400 MHz below).

1.042% and 0.73%, and the root mean square error (RMSE) is 0.013 and 0.016, respectively.

Figure 9 shows the regression analysis results of the BP neural network output at 200 MHz and 400 MHz. The correlation coefficients between the predicted and actual moisture content were 0.9254 and 0.9635, respectively, indicating that the method based on the combination of power spectral attribute parameters and BP neural network could reflect the nonlinear relationship between the power spectral attribute parameters of GPR and soil moisture content.

4. Field Measurement and Verification

In order to verify the validity of the numerical simulation results, the excavation profile of the Daliuta mining area (Fig. 10) was selected, and the surface soil was mainly eolian sand roadbed, and the 200 MHz frequency radar antenna was selected for detection. Samples were taken every 50 cm in the direction of the survey line and every 10 cm in depth using a ring knife. The mass moisture content of the

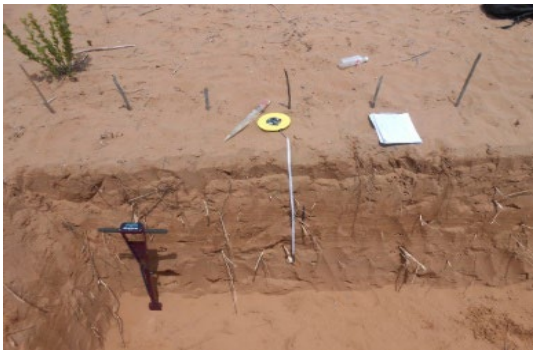

Fig. 10. Excavation profile site.

soil sample was measured by drying method in the laboratory, and then the soil volume moisture content was calculated according to the bulk density.

Firstly, the collected radar data was processed by zeroing, signal denoising and one-dimensional filtering. The early signal position was shown in Fig. 11, and the actual

single-channel waveform was transformed by Hilbert transform. The time window range corresponding to the first positive half cycle was read, the amplitude envelope was calculated, and the average amplitude envelope inverse value was obtained. The soil moisture content of the profile was calculated by using the conclusion in the numerical simulation (18).

Figure 12 was a comparison between the measured soil moisture content and the moisture content inverted by the AEA method. The absolute error is less than 0.9%, and the average error was 0.45%.

According to $h = 0.095 \times \exp[0.51/(\theta + 0.29)]$ (θ is the soil volume moisture content, h is the effective detection depth), the effective detection depth of the AEA method was calculated for each measurement point and the mean value was taken. The results showed that the AEA method can reach an effective detection depth of 0.41 m, and the calculated results were shown in Tab. 4.

The ARMA method was used to calculate the radar signal power spectrum. Then the radar signal power spectrum attribute parameters were calculated, and the correlation between them and soil moisture content and the independence between the attributes were analyzed. The rolling profile technique was used to segment according to the AEA effective detection depth. The preferred power spectrum attribute parameters for this field measurement verification were the main frequency, center frequency, frequency of the center of gravity, band energy, standard deviation of frequency, band energy share 0–200 MHz, band energy share 200–300 MHz.

According to the effective detection depth obtained by the AEA method, the radar signal corresponding to 20 ns was intercepted by the rolling spectrum profile technology, the time profile was converted into the power spectrum profile, and the corresponding power spectrum attribute parameters were calculated. The power spectrum attribute parameters of different measurement points and different depths of the excavation profile were selected as the test sample set, and the neural network parameters were adjusted during the continuous training process, and the number of hidden layers and nodes of the neural network were determined to be 3 layers, 10 nodes, learning efficiency of 0.15 and 30,000 training times, respectively. The power spectrum attribute parameters that were not involved in the training were used to invert the soil moisture content, and compared with the measured soil moisture content, the error (Fig. 13) and the network output regression line (Fig. 14) were analyzed.

The analysis showed that the error in the shallow range of 0–10 cm was greater than 1%, and the accuracy of 10–90 cm improved with the increase of depth, all less than 0.7%. Indicating that the inversion effect of soil moisture

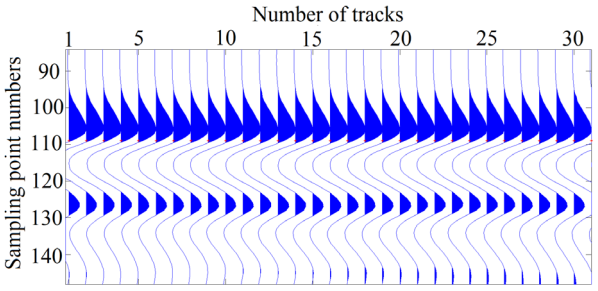

Fig. 11. Radar waveform of the excavation profile.

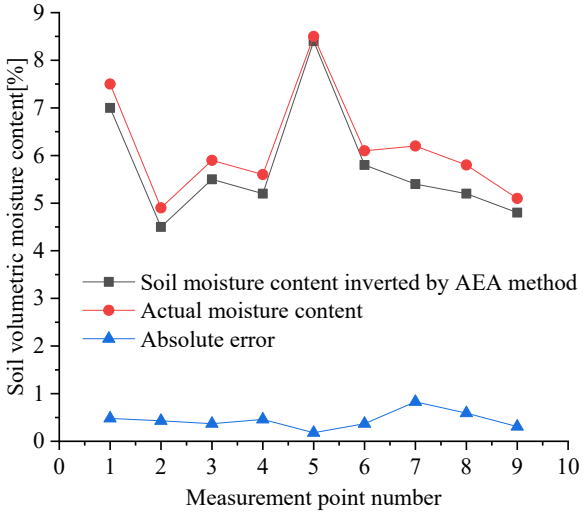

Fig. 12. Comparison of measured moisture content and soil moisture content inverted by AEA method.

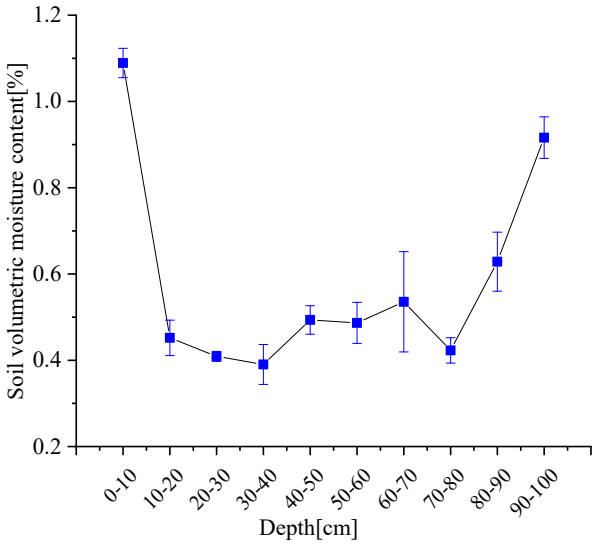

Fig. 13. Error analysis of soil moisture content inversion by radar power spectrum combined with BP neural network.

Measurement point number	1	2	3	4	5	6	7	8	9
H [m]	0.38	0.43	0.41	0.41	0.37	0.41	0.40	0.41	0.42
Average value [m]	0.41								

Tab. 4. Effective detection depths corresponding to different soil moisture contents.

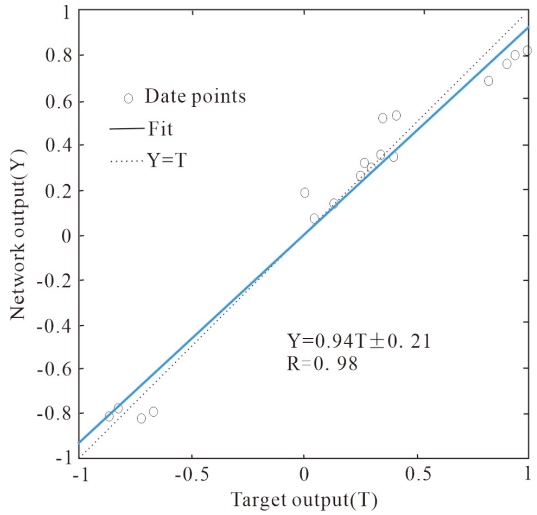

Fig. 14. Outdoor verification of GPR power spectrum combined with BP neural network output regression line.

content was better in this depth range. When the depth continues to increase to 90–100 cm, the absolute error showed a tendency to increase again, but does not exceed 1%. The overall results of the network output regression line analysis showed that the ARMA method combined with the BP neural network could successfully invert the soil moisture content in the range of 10–100 cm of the excavation profile.

5. Conclusions

In this paper, the methods of AEA and ARMA for inverting soil moisture content in the depth range that can be detected by ground penetrating radar were studied. By carrying out GPR numerical simulation and field measurement, the soil moisture content at different depths was inverted, and the following conclusions were drawn:

There was an obvious linear relationship between the reciprocal envelope of the early signal amplitude of GPR and the soil moisture content, and the relationship ($y = 2.540x - 0.007719$ ($R^2 = 0.987$)) between the early signal amplitude of AEA and the soil moisture content was given to reduce the error of secondary transmission. The relationship between the effective detection depth and the soil moisture content was as follows:
200 MHz: $h = 0.095 \times \exp[0.51/(\theta + 0.29)]$ ($R^2 = 0.999$);
400 MHz: $h = 0.068 \times \exp[0.38/(\theta + 0.26)]$ ($R^2 = 0.999$).

The combined ARMA method and BP neural network successfully inverted the soil moisture content at different depths in the field radar detection profile. The prediction accuracy in the shallow part of the first Gaussian window range was insufficient, and the error of soil moisture content inversion at the rest of the depths was less than 1.0%.

The experimental results showed that the AEA method is suitable for the detection of soil moisture content near the surface, while the ARMA method was suitable for the detection of soil moisture content in the middle and deep layers. Based on this, the AEA method and the ARMA method can complement each other's strengths, and the coupling of the two methods can invert the soil moisture content in the whole GPR detection depth range.

Acknowledgments

This research has been supported by the National Natural Science Foundation of China (No. 42264008). The authors express their gratitude to the valuable feedback provided by the reviewers and editors.

References

[1] LUNT, I. A., HUBBARD, S. S., RUBIN, Y. Soil moisture content estimation using ground-penetrating radar reflection data. *Journal of Hydrology*, 2005, vol. 307, no. 1–4, p. 254–269. DOI: 10.1016/j.jhydrol.2004.10.014

[2] ZHANG, R., CHEN, X., LU, P., et al. The effect of different mulching modes on soil moisture, temperature and yield of potato in dry land (in Chinese). *Crops*, 2023, no. 5, p. 145–150. DOI: 10.16035/j.issn.1001-7283.2023.05.021

[3] BENEDETTO, A. Water content evaluation in unsaturated soil using GPR signal analysis in the frequency domain. *Journal of Applied Geophysics*, 2010, vol. 71, no. 1, p. 26–35. DOI: 10.1016/j.jappgeo.2010.03.001

[4] LIU, Y., WEI, L. S., HUANG, A. B., et al. Temporal and spatial evolution of soil water in the source of the Yangtze river under climate change and its environmental response (in Chinese). *Hydrogeology & Engineering Geology*, 2023, vol. 50, no. 5, p. 39–52. DOI: 10.16030/j.cnki.issn.1000-3665.202301034

[5] DANIELS, D. J. *Ground Penetrating Radar*. 1st ed. London (UK): The Institution of Electrical Engineers, 2004. ISBN: 9780863413605

[6] ODEN, C. P., POWERS, M. H., WRIGHT, D. L., et al. Improving GPR image resolution in lossy ground using dispersive migration. *IEEE Transactions on Geoscience and Remote Sensing*, 2007, vol. 45, no. 8, p. 2492–2500. DOI: 10.1109/tgrs.2006.888933

[7] WANG, T., ORISTAGLIO, M. L. 3-D simulation of GPR surveys over pipes in dispersive soils. *Geophysics*, 2000, vol. 65, no. 5, p. 1560–1568. DOI: 10.1190/1.1444844

[8] HUISMAN, J. A., HUBBARD, S. S., REDMAN, J. D., et al. Measuring soil water content with ground penetrating radar: A review. *Vadose Zone Journal*, 2003, vol. 2, no. 4, p. 476–491. DOI: 10.2113/2.4.476

[9] KOYAMA, C. N., LIU, H., TAKAHASHI, K., et al. In-situ measurement of soil permittivity at various depths for the calibration and validation of low-frequency SAR soil moisture models by using GPR. *Remote Sensing*, 2017, vol. 9, no. 6, p. 1–14. DOI: 10.3390/rs9060580

[10] ERCOLI, M., DI MATTEO, L., PAUSELLI, C., et al. Integrated GPR and laboratory water content measures of sandy soils: From laboratory to field scale. *Construction and Building Materials*, 2018, vol. 159, p. 734–744. DOI: 10.1016/j.conbuildmat.2017.11.082

[11] PETTINELLI, E., VANNARONI, G., DI PASQUO, B., et al. Correlation between near-surface electromagnetic soil parameters and early-time GPR signals: An experimental study. *Geophysics*, 2007, vol. 72, no. 2, p. A25–A28. DOI: 10.1190/1.2435171

[12] DI MATTEO, A., PETTINELLI, E., SLOB, E. Early-time GPR signal attributes to estimate soil dielectric permittivity: A theoretical study. *IEEE Transactions on Geoscience and Remote Sensing*, 2012, vol. 51, no. 3, p. 1643–1654. DOI: 10.1109/tgrs.2012.2206817

[13] FERRARA, C., BARONE, P. M., STEELMAN, C. M., et al. Monitoring shallow soil water content under natural field conditions using the early-time GPR signal technique. *Vadose Zone Journal*, 2013, vol. 12, no. 4, p. 1–9. DOI: 10.2136/vzj2012.0202

[14] ALGEO, J., VAN DAM, R. L., SLATER, L. Early-time GPR: A method to monitor spatial variations in soil water content during irrigation in clay soils. *Vadose Zone Journal*, 2016, vol. 15, no. 11, p. 1–9. DOI: 10.2136/vzj2016.03.0026

[15] PETTINELLI, E., DI MATTEO, A., BEAUBIEN, S. E., et al. A controlled experiment to investigate the correlation between early-time signal attributes of ground-coupled radar and soil dielectric properties. *Journal of Applied Geophysics*, 2014, vol. 101, p. 68–76. DOI: 10.1016/j.jappgeo.2013.11.012

[16] COMITE, D., GALLI, A., LAURO, S. E., et al. Analysis of GPR early-time signal features for the evaluation of soil permittivity through numerical and experimental surveys. *IEEE Journal of Selected Topics in Applied Earth Observations and Remote Sensing*, 2015, vol. 9, no. 1, p. 178–187. DOI: 10.1109/jstars.2015.2466174

[17] WU, K., DESESQUELLES, H., COCKENPOT, R., et al. Ground-penetrating radar full-wave inversion for soil moisture mapping in trench-hill potato fields for precise irrigation. *Remote Sensing*, 2022, vol. 14, p. 1–16. DOI: 10.3390/rs14236046

[18] LAURENS, S., BALAYSSAC, J. P., RHAZI, J., et al. Non-destructive evaluation of concrete moisture by GPR: Experimental study and direct modeling. *Materials and Structures*, 2005, vol. 38, no. 9, p. 827–832. DOI: 10.1007/bf02481655

[19] ARDEKANI, M. R., NEYT, X., BENEDETTO, D., et al. Soil moisture variability effect on GPR data. In *Proceedings of the 15th International Conference on Ground Penetrating Radar.* Brussels (Belgium), 2014, p. 214–217. DOI: 10.1109/ICGPR.2014.6970416

[20] PONGRAC, B., GLEICH, D. Remote monitoring system based on cross-hole GPR and deep learning. In *2023 17th International Conference on Telecommunications (ConTEL).* Graz (Austria), 2023, p. 1–5. DOI: 10.1109/ConTEL58387.2023.10198933

[21] YANG, F., ZHANG, Q. S., WANG, P. Y. *Research on Geological Radar Detection Technology for Highway Roadbeds* (in Chinese). Beijing (China): China Communication Press, 2009. ISBN: 9787114079115

[22] CUI, F., WU, Z. Y., WANG, L., et al. Application of the ground penetrating radar ARMA power spectrum estimation method to detect moisture content and compactness values in sandy loam. *Journal of Applied Geophysics*, 2015, vol. 120, p. 26–35. DOI: 10.1016/j.jappgeo.2015.06.006

[23] CHENG, Q., ZHANG, S. W., LUO, M., et al. Inversion of reclaimed soil moisture based on ground penetrating radar fly ash filling (in Chinese). *Progress in Geophysics*, 2021, vol. 36, no. 5, p. 2159 to 2167. DOI: 10.6038/pg2021EE0413

[24] WU, Z. Y., DU, W. F., NIE, J. L., et al. Detection of cohesive soil moisture content based on early signal amplitude envelope values of ground penetrating radar (in Chinese). *Transactions of the Chinese Society of Agricultural Engineering*, 2019, vol. 35, no. 22, p. 115–121. DOI: 10.11975/j.issn.1002-6819.2019.22.013

[25] XIE, G. Q., NIE, J. L., CHEN, Z. Q., et al. Prediction of soil moisture status based on ground penetrating radar power spectrum attribute parameters (in Chinese). *Water Saving Irrigation*, 2023, no. 10, p. 28–35. DOI: 10.12396/jsgg.2023147

[26] TANG, M. G., QI, M., WANG, D. J., et al. Application of ARMA model in accuracy analysis of radar dynamic measurement (in Chinese). *Modern Radar*, 2019, vol. 41, no. 5, p. 77–81. DOI: 10.16592/j.cnki.1004-7859.2019.05.015

[27] WANG, F. Y., ZHANG, L. L. Power spectrum estimation and MATLAB simulation (in Chinese). *Microcomputer Information*, 2006, no. 31, p. 287–289. DOI: 10.3969/j.issn.1008-0570.2006.31.102

[28] GIANNOPOULOS, A. Modelling ground penetrating radar by GprMax. *Construction and Building Materials*, 2005, vol. 19, no. 10, p. 755–762. DOI: 10.1016/j.conbuildmat.2005.06.007

[29] STEELMAN, C. M., ENDRES, A. L. An examination of direct ground wave soil moisture monitoring over an annual cycle of soil conditions. *Water Resources Research*, 2010, vol. 46, no. 11, p. 1–16. DOI: 10.1029/2009wr008815

[30] DONG, L., WANG, L. J., HAO, Y., et al. Wind power generation capacity prediction based on autoregressive moving average model (in Chinese). *Acta Energiae Solaris Sinica*, 2011, vol. 32, no. 5, p. 617–622. ISSN: 0254-0096

[31] ZHU, M. T., LIU, J., WANG, G. L. Research on the order determination method of AR model for road surface irregularity reconstruction (in Chinese). *Journal of Highway and Transportation Research and Development*, 2010, vol. 27, no. 7, p. 25–28+51. DOI: 10.3969/j.issn.1002-0268.2010.07.005

About the Authors…

Yanling FENG was born in Hubei. She graduated from the School of Geophysics and Petroleum Resources of Yangtze University with a bachelor's degree in Engineering in 2021. She is currently pursuing a master's degree in Geological Resources and Geological Engineering from Guizhou University. Her research interests include soil water content retrieval based on ground penetrating radar technology.

Junli NIE (corresponding author) received her Ph.D. from the China University of Mining and Technology (Beijing) in 2011. She is currently an Associate Professor at Key Laboratory of Karst Georesources and Environment (Guizhou University), Ministry of Education, focusing on the application of geological radar.

Guoqing XIE received his master's degree in Geological Resources and Geological Engineering from Guizhou University in 2023. His current research direction is engineering geophysical exploration.

Heng LV received a master's degree in Geological Resources and Geological Engineering from Guizhou University in 2021.